Biomolecular NMR Assignments
https://doi.org/10.1007/s12104-024-10180-8

ARTICLE

Resonance assignments of cytochrome MtoD from the extracellular electron uptake pathway of *sideroxydans lithotrophicus* ES-1

Anaísa Coelho[1] · José M. Silva[2,3] · Francesca Cantini[2,3] · Mario Piccioli[2,3] · Ricardo O. Louro[1] · Catarina M. Paquete[1]

Received: 19 April 2024 / Accepted: 31 May 2024

Abstract
The contribution of Fe(II)-oxidizing bacteria to iron cycling in freshwater, groundwater, and marine environments has been widely recognized in recent years. These organisms perform extracellular electron transfer (EET), which constitutes the foundations of bioelectrochemical systems for the production of biofuels and bioenergy. It was proposed that the Gram-negative bacterium *Sideroxydans lithotrophicus* ES-1 oxidizes soluble ferrous Fe(II) at the surface of the cell and performs EET through the Mto redox pathway. This pathway is composed by the periplasmic monoheme cytochrome MtoD that is proposed to bridge electron transfer between the cell exterior and the cytoplasm. This makes its functional and structural characterization, as well as evaluating the interaction process with its physiological partners, essential for understanding the mechanisms underlying EET. Here, we report the complete assignment of the heme proton and carbon signals together with a near-complete assignment of ^{1}H, ^{13}C and ^{15}N backbone and side chain resonances for the reduced, diamagnetic form of the protein. These data pave the way to identify and structurally map the molecular interaction regions between the cytochrome MtoD and its physiological redox partners, to explore the EET processes of *S. lithotrophicus* ES-1.

Keywords NMR resonance assignment · Cytochromes · MtoD · Extracellular electron transfer · Ring current shifts

Biological context

Fe(II)-oxidizing bacteria play an important role in numerous biogeochemical cycles, including that of iron (Kappler and Straub 2005), and are currently being explored for the development of biotechnological processes such as bioelectrosynthesis where microbial metabolism is driven directly by electricity (Gupta et al. 2020; Karthikeyan et al. 2019; Summers et al. 2013). In their natural environments, these organisms perform extracellular electron transfer (EET), taking up electrons from Fe(II) outside of the cell, and transferring them to the quinone pool in the inner membrane. These pathways connect extracellular redox reactions to intracellular metabolic activity and are made up of redox and structural proteins that work together to transfer electrons between extracellular substrates and the cytoplasmic membrane (Bird et al. 2014; Jain et al. 2022b; Liu et al. 2012; Valdés et al. 2008; Zhou et al. 2022).

Although several Fe(II) oxidizers have been identified, the understanding of the electron transfer mechanisms involved in growth and energy conservation in Fe(II)-oxidizing bacteria lags far behind. This is primarily due to difficulties encountered in culturing various of these microorganisms that achieve only poor cell yields, as well as the lack of genetic systems for their manipulation in many cases (Ilbert and Bonnefoy 2013).

Sideroxydans lithotrophicus ES-1 is a freshwater chemolithoautotrophic Gram-negative bacterium able to oxidize Fe(II) at the cell surface. It was proposed that this organism relies on different pathways to perform EET, including the Mto pathway (Jain et al. 2022b; Zhou et al. 2022). In this pathway, it is proposed that the monoheme cytochrome

✉ Mario Piccioli
piccioli@cerm.unifi.it

✉ Ricardo O. Louro
louro@itqb.unl.pt

[1] Instituto de Tecnologia Química e Biológica António Xavier (ITQB-NOVA), Universidade Nova de Lisboa, Av. da República (EAN), Oeiras 2780-157, Portugal

[2] Department of Chemistry, Magnetic Resonance Center (CERM), University of Florence, Via L. Sacconi 6, Sesto Fiorentino 50019, Italy

[3] Consorzio Interuniversitario Risonanze Magnetiche MetalloProteine (CIRMMP), Via L. Sacconi 6, Sesto Fiorentino 50019, Italy

Published online: 07 June 2024

MtoD shuttles electrons across the periplasmic space, between the outer membrane-associated decaheme cytochrome-porin complex MtoAB and the inner membrane oxidoreductase ImoA, a tetraheme cytochrome that belongs to the NapC/NirT family (Jain et al. 2022a, b). MtoA and MtoB are homologs of MtrA and MtrB, respectively. These proteins belong to the MtrCAB complex from the Fe(III)-reducing Gram-negative bacterium *Shewanella oneidensis* MR-1, known to be involved in efficient electron transport across the outer membrane (Zhong and Shi 2018). ImoA has been proposed to function as the quinone oxidoreductase during Fe(II) oxidation based on its sequence similarity with the tetraheme cytochrome CymA from *S. oneidensis* MR-1 (Liu et al. 2012). The gene coding for MtoA, MtoB, MtoD and ImoA are all clustered together, indicating that their protein products likely work collectively to facilitate electron transfer across the cell envelope (He et al. 2017; Liu et al. 2012). It has been demonstrated that these proteins exhibit modularity, incorporating elements from other porin-cytochrome pathways, including those identified in *S. lithotrophicus* ES-1 (Jain et al. 2022b; Zhou et al. 2022). This suggests that this organism relies on multiple interconnected EET pathways to facilitate Fe(II) oxidation (Jain et al. 2022b).

MtoD is a 117 amino acids monoheme *c*-type cytochrome that belongs to the class I of cytochromes *c* predicted to be located in the periplasm. Residues 1–27, forming the signal peptide, are cleaved and the mature protein, containing a Strep-II affinity tag, is a 98 aminoacids, 11 kDa protein. The atomic structure of this protein in the oxidized state was determined by X-ray crystallography. It revealed the *c*-type heme cofactor axially coordinated by two histidine residues, which is an uncommon feature for this class of cytochromes (Beckwith et al. 2015). The unusual bis-His axial heme ligation gives MtoD a lower reduction potential (155 ± 10mV (Beckwith et al. 2015) than typically observed for class I cytochromes *c* ($\sim +200$ to $+250$ mV). To validate the proposed pathway and verify that MtoD can receive electrons from MtoA and transfer them to ImoA, interaction studies must be performed. NMR spectroscopy is a powerful technique to explore transient complexes and weak protein–protein interactions (Fonseca et al. 2013; Piccioli and Turano 2015; Ubbink 2012), providing both dynamic and structural information in different oxidation states of redox proteins in solution at atomic resolution (Fonseca et al. 2013; Morgado and Salgueiro 2022). However, to achieve this, a full assignment of the NMR signals of MtoD is mandatory not only to study interactions between MtoD and physiological partner proteins, but also to identify the interacting regions at the surface of MtoD. In this work, the complete assignment of the heme proton and carbon signals and a near-complete assignment of ^{1}H, ^{15}N and ^{13}C backbone and side chain resonances for MtoD containing a Strep-II affinity tag was obtained for the reduced, diamagnetic, form of the protein. This information will be essential to understand the role of MtoD in the EET processes in *S. lithotrophicus* ES-1.

Methods and experiments

Construction of bacterial strains

Strains, primers and plasmids used in this study are listed in Table 1. The gene *mtoD* was kindly provided by Thomas A. Clarke from the University of East Anglia, Norwich, UK. The sequence of the signal peptide derived from the periplasmic monoheme cytochrome MtoD from *S. lithotrophicus* ES-1 was replaced by the sequence of the signal peptide of OmpA from *E. coli*. The DNA fragment coding for OmpA was amplified from the genomic DNA of *E. coli* (DH5α)

Table 1 Bacterial strains, plasmids, and primers used in this study

Strains, plasmids, primers	Relevant characteristics	Source
Strains		
E. coli DH5α	Host for cloning	IBN Lab Strains Collection
E. coli JM109(DE3)	*E. coli* strain co-transformed with vector pEC86, which contains the *ccmABCDEFGH* genes	IBN Lab Strains Collection
Plasmids		
pBAD202/D-TOPO	Expression vector, Km^r	Invitrogen
pBAD202::*mtoD*	pBAD202/D-TOPO containing the OmpA signal peptide from *E. coli*, the *mtoD* gene and a Strep-II tag sequence.	This study
Primers	***Sequence (5' to 3')***	
Primer 1	GAGATATACATACCATGAAAAAGACAGCTATCGCGATTGC	This study
Primer 2	CAGCGTCGACATCGACAGCTGCCTGCGCAACGGTAGC	This study
Primer 3	GCTACCGTTGCGCAGGCAGCTGTCGATGTCGACGCTG	This study
Primer 4	TATCAGATCCCATGCTACTTCTCGAATTGTGGATGAGAC	This study

using primers 1 and 2, while the MtoD protein with the Strep-II tag was amplified using primers 3 and 4 (Table 1). The OmpA and MtoD fragments were purified and cloned in the NcoI restriction site of the pBAD202/D-TOPO vector (Invitrogen, Carlsbad, CA, USA) using the NEBuilder Assembly kit (New England BioLabs). The resulting plasmid (pBAD202::*mtoD*) was transformed into chemically competent *E. coli* strain JM109(DE3) co-transformed with vector pEC86, which contains the *ccmABCDEFGH* genes (Thöny-Meyer et al. 1995).

Protein expression and purification

MtoD (*mtoD* gene containing a Strep-II tag – residues 28–117 and residues 118–125, respectively) was produced as unlabeled, single ^{15}N-labeled, uniform double ^{15}N,^{13}C-labeled and selective-unlabeled ^{15}N-labeled samples. The *E. coli* strains JM109(DE3) harboring pEC86 and pBAD202::*mtoD* were grown aerobically at 37 ºC in Lysogeny Broth (LB) medium containing 50 μg/cm^3 kanamycin and 34 μg/cm^3 chloramphenicol in 5.0 dm^3 Erlenmeyer flasks containing 2.0 dm^3 of medium at 150 rev./min to an optical density (OD_{600nm}) of 1.0. This culture was then processed as follow: (a) to produce unlabeled MtoD: 10 mM L-arabinose was added and the cells were allowed to grow under the same conditions for 8 h before harvesting; (b) to produce ^{15}N-MtoD: the cells were collected by centrifugation, washed twice with 250 cm^3 of a salt solution containing 12.8 g/dm^3 Na_2HPO_4, 3.0 g/dm^3 KH_2PO_4 and 0.50 g/dm^3 NaCl, resuspended in minimal media (in a ratio of 250 cm^3 of minimal medium for each dm^3 of LB medium) supplied with 1.0 g/dm^3 of ammonium sulfate ($^{15}N_2$, 99%) as nitrogen source, (together with 2 mM $MgSO_4$, 0.1 mM $CaCl_2$, 0.05 mM $FeSO_4$ and 0.2 g/L yeast extract), grown for 8 h at 37 ºC in the presence of 10 mM L-arabinose and harvested by centrifugation; (c) to produce uniform ^{15}N,^{13}C-MtoD: as described in (b) but also supplied with 2.0 g/dm^3 [U–$^{13}C_6$] D-glucose as carbon source; (d) to produce selective-unlabeled ^{15}N-MtoD: as described in (b) but each growth also supplied with one of four different amino acids in an unlabeled form (Asn, Cys, His or Lys, at 1.0 g/ dm^3).

All bacterial cells were harvested by centrifugation at 10,000 *g* for 15 min at 4 ºC. The cell pellet was resuspended in 100 mM Tris-HCl (pH 7.4) containing EDTA-free protease inhibitor cocktail (Roche) and DNase I (Sigma). The disruption of the cells was achieved by three passages through a French Press at a pressure of 1,000 psi (6.89 MPa). The crude extract was centrifuged at 200,000 g for 1 h at 4 ºC (Beckman Coulter Optima LE-80 K). The supernatant containing the soluble protein fraction was loaded into a 5 mL Strep-Tactin® column (IBA) previously equilibrated with 100 mM Tris-HCl, pH 7.4, 150 mM NaCl and the protein was eluted using Elution Buffer (100 mM Tris-HCl, pH 7.4, 150 mM NaCl, 2.5 mM desthiobiotin). Eluted fractions were analyzed by SDS-PAGE (12% gel) stained for heme proteins (Francis and Becker, 1984) and BlueSafe. The purity index of the sample was defined by the $A_{Soret\ peak}/A_{280nm}$ ratio using UV-visible spectroscopy measurements. The final purified MtoD was concentrated at 4 ºC using an Amicon Ultra Centrifugal Filter (Millipore) with a 5 kDa cutoff. Protein concentration was estimated using the absorption coefficient, ε_{409nm}, of 125,000 $M^{-1}cm^{-1}$ per heme for the oxidized state of the protein (Massey 1959).

NMR experiments

Samples for NMR experiments with concentrations between 0.1 and 1.5 mM were prepared in ^2H_2O (99.9% atom) and 90% H_2O / 10% ^2H_2O (99.9 atom %). To obtain the fully reduced state of the protein, small amounts of solid sodium dithionite were added to the sample, in an argon atmosphere. NMR experiments were performed at 298 K on a NEO 500 MHz NMR spectrometer (Bruker, Rheinstetten, Germany) equipped with a 5 mm TCI C/N prodigy cryoprobe, on a Bruker Avance 800 MHz and on a Bruker 950 MHz spectrometers equipped with a helium cold TCI cryoprobe, and on a Bruker 1,200 MHz spectrometer equipped with a TXO 5 mm cryoprobe. Assignment of the proton heme signals was performed using a 0.1 mM sample of unlabeled MtoD lyophilized twice using ^2H_2O (99.9 atom%) prepared in 20 mM potassium phosphate buffer at pH 7.6 with 80 mM NaCl. NMR spectra obtained before and after the lyophilization were identical, showing that the protein integrity was not affected by the procedure. 2D-nuclear Overhauser effect spectroscopy (NOESY) (50, 200 and 400 ms, mixing time) spectra and 2D-total correlation spectroscopy (TOCSY) (60 ms mixing time) spectra were collected. For backbone and side chain assignments, single ^{15}N-labeled, uniform double ^{15}N,^{13}C-labeled, and selective-unlabeled ^{15}N-labeled samples with concentrations between 0.1 and 1.5 mM were prepared in 20 mM potassium phosphate buffer at pH 6.5 with 50 mM NaCl. A set of double and triple resonance experiments was performed: (i) ^{13}C- and ^{15}N-HSQC and HSQC-NOESY, HNCA, HNCO, HNCACO, CBCA(CO)NH, CBCANH, HNHA, HCCH-TOCSY (Cavanagh et al. 2007) for ^{15}N,^{13}C-MtoD sample and (ii) ^{15}N-HSQC for the ^{15}N-MtoD and selective-unlabeled ^{15}N-MtoD (Table S1). ^{1}H chemical shifts were calibrated using the water signal as an internal reference and both ^{13}C and ^{15}N chemical shifts were calibrated through indirect referencing (Wishart et al. 1995). All NMR spectra were processed using Topspin 4.1.1 software (Bruker Biospin, Karlsruhe, Germany). Sparky (TD Goddard and DG Kneller, Sparky 3, University of California, San Francisco, USA) was used for heme assignment

and CARA (Keller 2004) was used for the backbone and side chain assignments.

Results

Extent of assignments and data deposition

Production of MtoD

The production of *c*-type cytochromes requires specific cell machinery, such as the cytochrome *c* maturation system and Sec translocation system (Verissimo and Daldal 2014). To ensure that the target protein MtoD is recognized by the *E. coli* Sec translocation system, the signal peptide of OmpA was used. It is known that the outer-membrane protein OmpA from *E. coli* is constitutively expressed in high levels in *E. coli* under aerobic conditions, containing the ideal signal peptide for the heterologous expression of proteins, including MtoD (Low et al. 2013). To facilitate the purification process, the protein was engineered to carry a C-terminal Strep-II affinity tag. SDS-PAGE analysis confirmed the purity of MtoD, running as a single band with an apparent molecular weight of 11 kDa (Figure S1A) and staining positively for the covalent attachment of the heme (Figure S1B). Pure MtoD presented an absorbance ratio of $A_{\text{Soret Peak}}/A_{280\text{nm}}$ of 5 (Figure S1C).

NMR assignments

Assignment of heme resonances

To properly map the interacting docking regions within a redox complex established with MtoD, it is necessary to assign the protein's backbone NMR signals and the heme substituent NMR signals. The crystal structure of MtoD previously determined (Beckwith et al. 2015), reveals that the heme has bis-histidinyl axial coordination. Given the differences between the spin state of the system (i.e. diamagnetic (Fe(II), S = 0) in the reduced state and paramagnetic (Fe(III), S = 1/2) in the oxidized state) (Querci et al. 2024; Trindade et al. 2022), 1D ^{1}H NMR spectra of cytochrome MtoD display distinct features in the reduced and oxidized states (Fig. 1). In the reduced state, the signals are sharp and spread over the 10 to − 1 ppm region, while in the oxidized state the signals are broader and span a wider spectral region ranging from 29 to − 2 ppm. In fact, because the heme is diamagnetic in the reduced state, the signals of the heme substituents can be observed in typical regions: 9 − 10 ppm for meso protons (H5, H10, H15, and H20, according to the IUPAC-IUB nomenclature for tetrapyrroles (Figure S2); 5 − 7 ppm for thioether methines (H3^{1} and H8^{1}); 2 − 4 ppm for methyl groups (M2^{1}, M7^{1}, M12^{1}, and M18^{1}); and 1 − 3 ppm for thioether methyls (M3^{2} and M8^{2}) (Silva and Louro 2017).

The heme proton signals were assigned using the 2D ^{1}H NMR spectra (NOESY and TOCSY) acquired for the non-labeled sample prepared in $^{2}H_2O$, as previously described (Silva and Louro 2017) (Figure S3). The carbon signals were assigned using the 2D ^{1}H,^{13}C-HSQC and 3D ^{13}C-edited [^{1}H,^{1}H]-NOESY spectra. The assignment of the heme signals is shown in Table 2.

Assignment of protein resonances

The combined analysis of 2D ^{1}H,^{15}N-HSQC and the series of 3D NMR spectra (3D CBCANH, 3D CBCA(CO)NH, 3D HNCO, 3D HNCA, 3D HNCACO) led to the near-complete

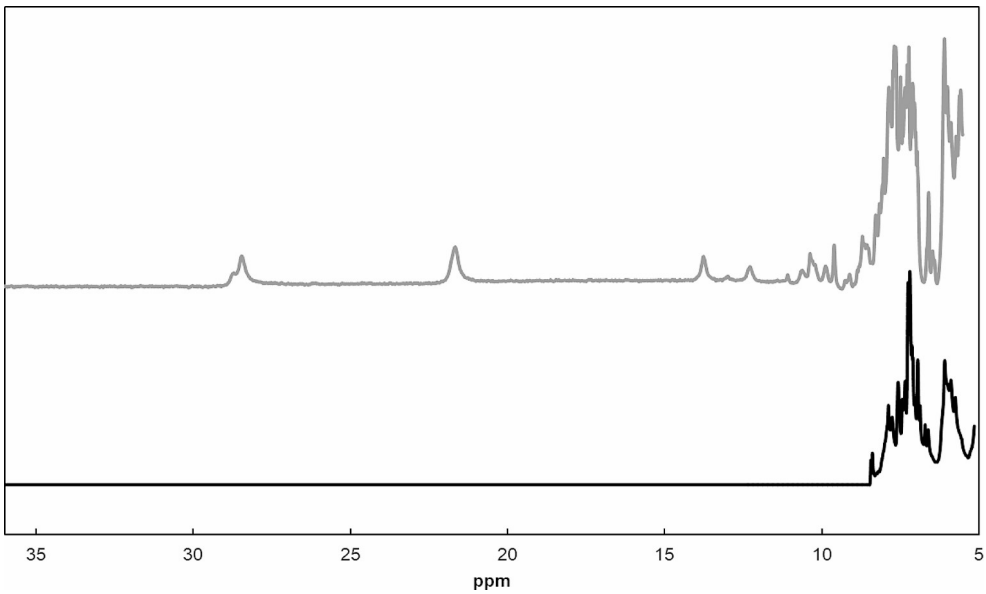

Fig. 1 ^{1}H NMR spectra of cytochrome MtoD in the reduced and oxidized state downfield of the residual solvent water signal. Spectrum in the reduced state (black line) was obtained by the addition of small amounts of sodium dithionite to the oxidized (gray line) sample

Table 2 Assignment of proton and carbon NMR resonances of the heme substituents of MtoD. The heme substituents are numbered according to the IUPAC-IUB nomenclature (Figure S2)

Substituent	Chemical shifts of heme protons (ppm)	Substituent	Chemical shifts of heme carbons (ppm)
H5	9.43	CAA	26.09
H10	8.88	CAB	34.84
H15	9.57	CAC	38.54
H20	9.17	CAD	25.21
$M2^1$	3.25	CBB	24.32
$M7^1$	3.64	CBC	22.31
$M12^1$	2.52	CBD	44.87
$M18^1$	3.53	CHA	99.76
$H3^1$	5.82	CHB	99.12
$H8^1$	6.14	CHC	100.75
$M3^2$	1.87	CHD	100.73
$M8^2$	2.2	CMA	14.86
$P17^1{}_1$	4.26	CMB	15.02
$P17^1{}_2$	3.51	CMC	15.02
$P13^1{}_1$	4.34	CMD	11.18
$P13^1{}_2$	3.82		
$P13^2{}_1$	3.27		
$P13^2{}_2$	2.92		

assignment of backbone ^{15}N (94%), $^{1}H_N$ (98%), $^{13}C_\alpha$ (100%), $^{13}C_\beta$ (100%) and ^{13}CO (97%). The only residues unobserved in the ^{15}N HSQC experiment were Lys 45 and Lys 84. Figure 2 shows the 2D ^{1}H,^{15}N-HSQC NMR spectrum of labeled MtoD with the HN assignments of backbone and side chains of asparagine (N41, N42, N97, N99, N109) and glutamine (Q122) residues.

The 2D ^{1}H,^{13}C-HSQC spectrum, combined with 3D HCC(H) TOCSY spectrum, allowed the assignment of the aliphatic protons and remaining aliphatic carbon signals of the protein ($^{1}H_\alpha$, $^{1}H_\beta$, $^{1}H_\gamma$, $^{1}H_\delta$, $^{1}H_\varepsilon$ and $^{13}C_\gamma$, $^{13}C_\delta$, $^{13}C_\varepsilon$). The total extent of the assignment for the ^{1}H, ^{13}C and ^{15}N, is 83%, 83% and 82%, respectively. The ^{1}H, ^{13}C and ^{15}N chemical shifts have been deposited in the BioMagResBank (http://www.bmrb.wisc.edu) under BMRB accession number 51671.

Analysis of chemical shifts

The ring-current effects generated by the heme group are significantly stronger than those produced by the amino acid aromatic side chains. Consequently, the nuclei located close to the heme group are subject to a strong ring-current contribution on their observed shifts and may significantly deviate from the expected values. The most affected nuclei are those belonging to the axial histidine. In fact, the His $H_{\beta2}$ and $H_{\beta1}$, and H_α signals are strongly up-field shifted appearing in the −0.12–1.39 ppm and 2.83–3.20 ppm range, respectively, with sizable deviations from the values that are typically found in the absence of heme-ring current shifts (around 2.7–3.5 ppm for H_β and around 4.2–5.0 ppm for H_α). The

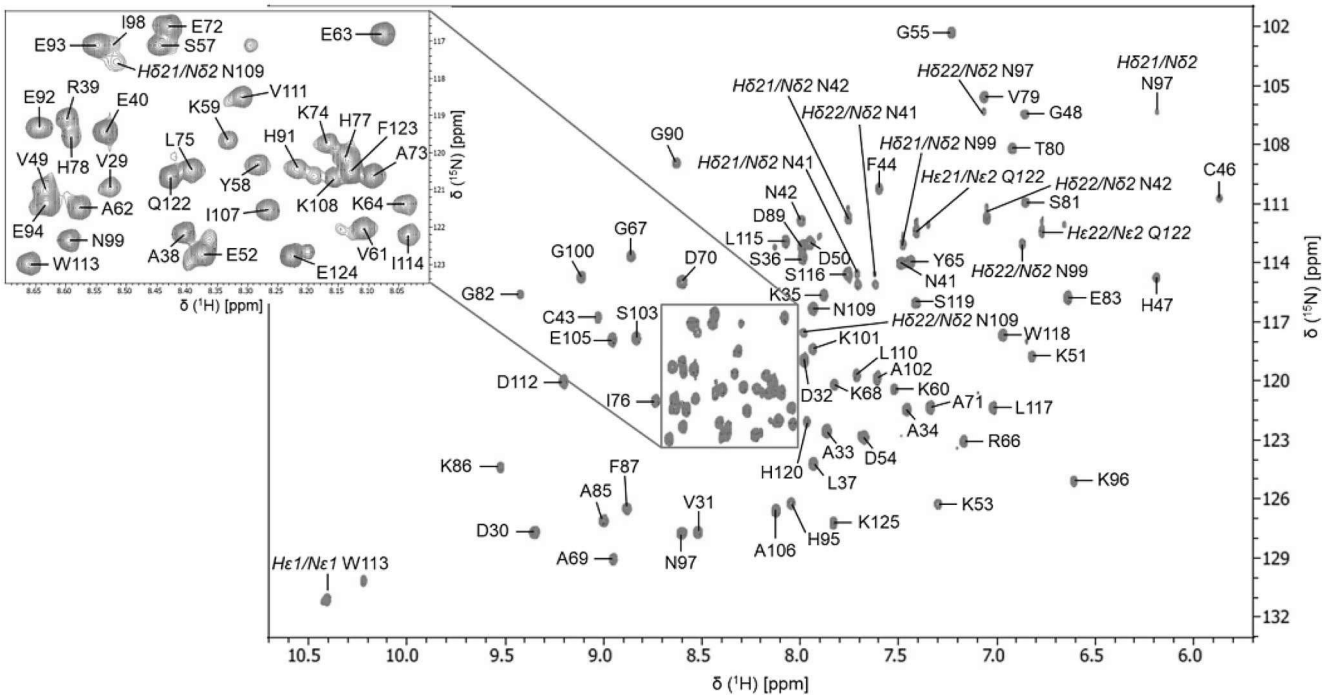

Fig. 2 ^{15}N,^{1}H-HSQC spectrum of MtoD. The spectrum was recorded at a proton resonance frequency of 800 MHz at 298 K, in 20 mM potassium phosphate buffer (90% H_2O / 10% $^{2}H_2O$) at pH 6.5 with 50 mM NaCl concentration. Resonance assignments are labelled in black according to the native sequence of MtoD. The insert expands the more crowded region of the spectrum

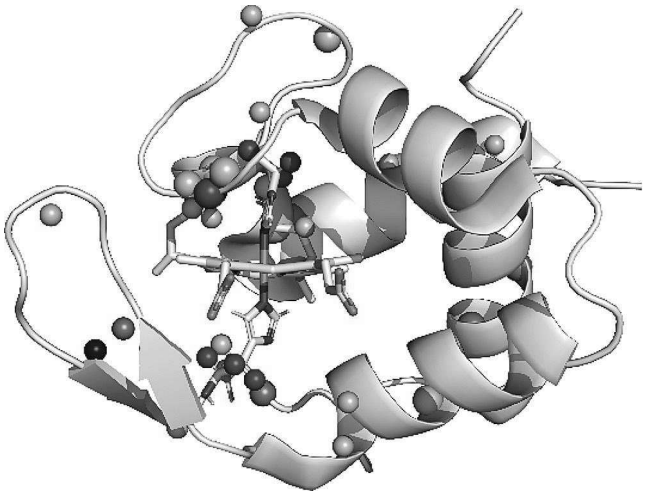

Fig. 3 Chemical shifts deviating from the statistics reported in the BMRB database shown in the crystallographic protein structure. Atoms deviating from the average shift by more than two standard deviation values are, respectively, shown in light blue (positive shift) and pink (negative shift); atoms deviating by more than three standard deviation values are, respectively, shown in blue (positive shift) and red (negative shift). A larger sphere radius was used for heteroatoms

chemical shifts of other nuclei located in the neighborhood of the heme group are also significantly affected as is the case of Cys 43 H_β, Cys 46 H_N and H_β, Gly 48 H_N, Lys 96 H_N, H_α, H_β, and H_ε, which experience a shielding effect with respect to the random coil values. Since the monoheme cytochrome MtoD is relatively small (11 kDa), most nuclei are located in the vicinity of the heme group, and therefore this effect is extended to the proton, nitrogen, and carbon atoms of other amino acids. Indeed, Fig. 3 shows, for overall backbone atoms and for the side chains of heme bound residues, atoms with shifts that deviate from the expectation values (https://bmrb.io/ref_info/csstats.php?restype=aa&set=filt) .

The observed chemical shifts of nuclei located in the vicinity of the heme group are affected differently, depending on their distance from the heme and position relative to the heme plane (Cross and Wright 1985; Johnson and Bovey 1958). Consistent with the structure of the heme pocket, a predominance of shielding contributions are observed along the bis-histidine axis of the system.

Despite the caveat of the effect of the heme ring current shifts, the spectral position of the assigned backbone signals was then used to predict the protein secondary structure elements in solution using the TALOS + software (Shen et al. 2009) (Fig. 4). The data indicate that the dominant secondary structural elements in this protein are α-helices. The prediction closely matches that of the crystal structure of the protein (Beckwith et al. 2015).

Conclusion

The complete assignment of the heme proton and carbon (quaternary) signals together with a near-complete assignment of ^{1}H, ^{13}C and ^{15}N backbone and side chain resonances obtained in the present work constitute important foundations to investigate and structurally map the interactions between MtoD and physiological partners. NMR-based biomolecular interaction studies between MtoD and its redox partners will contribute to characterize the molecular choreography that underpins the EET pathway of *S. lithotrophicus* ES-1, a knowledge that is still lacking in the quest to understand the biogeochemical cycling of metals in the environment.

Supplementary Information The online version contains supplementary material available at https://doi.org/10.1007/s12104-024-10180-8.

Acknowledgements This work benefited from access to CERM/CIRMMP, the Instruct-ERIC Italy center, and CERMAX, ITQB-NOVA, Oeiras, Portugal with equipment funded by FCT - Fundação para a Ciência e a Tecnologia, I.P. (FCT), project AAC 01/SAICT/2016. Financial support was provided by European EC Horizon2020 TIMB3 (Project 810856) Instruct-ERIC (PID22135). Financial support was also provided by Project MOSTMICRO-ITQB with refs UIDB/04612/2020 and UIDP/04612/2020, and projects PTDC/BIA-BQM/4143/2021 and PD/BD/135153/2017 integrated in the PhD Programme in NMR applied to chemistry, materials and biosciences

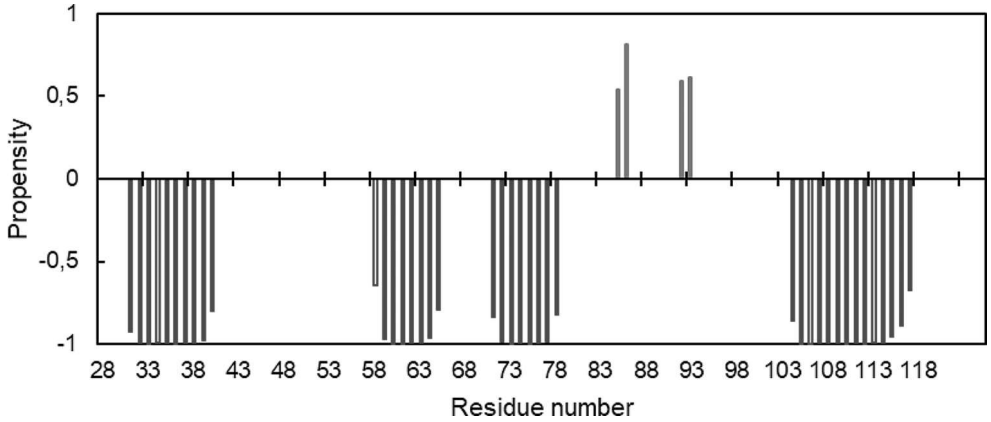

Fig. 4 Secondary structure elements of MtoD predicted by TALOS + software. α-helices are in red, β-strands in blue and the loop segments are not shown

(PD/00065/2013).

Author contributions A.C and J.M.S. performed and analyzed the experiments and wrote the main manuscript text F.C., M.P., R.O.L. and C.M.P. conceptualized the research and supervised the experiments. All authors reviewed the manuscript.

Funding Open access funding provided by Università degli Studi di Firenze within the CRUI-CARE Agreement.

Data availability Assignment deposited in BMRB, ID 51671.

Declarations

Conflict of interest The authors declare no competing financial interest.

References

Beckwith CR, Edwards MJ, Lawes M, Shi L, Butt JN, Richardson DJ, Clarke TA (2015) Characterization of MtoD from *sideroxydans lithotrophicus*: a cytochrome *c* electron shuttle used in lithoautotrophic growth. *In* Front Microbiol. 6

Bird LJ, Saraiva IH, Park S, Calcada EO, Salgueiro CA, Nitschke W, Louro RO, Newman DK (2014) Nonredundant roles for cytochrome c_2 and two high-potential iron-sulfur proteins in the photoferrotroph *Rhodopseudomonas palustris* TIE-1. J Bacteriol Vol 196:850–858. https://doi.org/10.1128/JB.00843-13. *In*

Cavanagh J, Fairbrother WJ, Palmer AG III, Rance M, Skelton NJ (2007) Protein NMR spectroscopy. Academic, Principles and practice SanDiego

Cross KJ, Wright PE (1985) Calibration of ring-current models for the heme ring. *In* Journal of Magnetic Resonance (1969). Vol. 64. Pp. 220–231 https://doi.org/10.1016/0022-2364(85)90346-4

Fonseca BM, Paquete CM, Neto SE, Pacheco I, Soares CM, Louro RO (2013) Mind the gap: cytochrome interactions reveal electron pathways across the periplasm of *Shewanella oneidensis* MR-1. Biochem J Vol 449:101–108. https://doi.org/10.1042/bj20121467. *In*

Gupta D, Guzman MS, Bose A (2020) Extracellular electron uptake by autotrophic microbes: physiological, ecological, and evolutionary implications. J Industrial Microbiol Biotechnol Vol 47:863–876. https://doi.org/10.1007/s10295-020-02309-0. *In*

He S, Barco RA, Emerson D, Roden EE (2017) Comparative genomic analysis of neutrophilic iron(II) oxidizer genomes for candidate genes in extracellular electron transfer. *In* Front Microbiol. 8

Ilbert M, Bonnefoy V (2013) Insight into the evolution of the iron oxidation pathways. *In* Biochim Biophys Acta. Vol. 1827. Pp. 161–75 https://doi.org/10.1016/j.bbabio.2012.10.001

Jain A, Coelho A, Madjarov J, Paquete CM, Gralnick JA (2022a) Evidence for quinol oxidation activity of ImoA, a novel NapC/NirT family protein from the neutrophilic Fe(II)-oxidizing bacterium *Sideroxydans lithotrophicus* ES-1. *In* mBio. Vol. 13. Pp. e0215022 https://doi.org/10.1128/mbio.02150-22

Jain A, Kalb MJ, Gralnick JA (2022b) Reconstructing electron transfer components from an Fe(II) oxidizing bacterium. *In* Microbiology. Vol. 168 https://doi.org/10.1099/mic.0.001240

Johnson CE Jr., Bovey FA (1958) Calculation of nuclear magnetic resonance spectra of aromatic hydrocarbons. J Chem Phys 29:1012–1014. https://doi.org/10.1063/1.1744645

Kappler A, Straub KL (2005) Geomicrobiological cycling of iron. *In* Reviews in Mineralogy and Geochemistry. Vol. 59. Pp. 85–108 https://doi.org/10.2138/rmg.2005.59.5

Karthikeyan R, Singh R, Bose A (2019) Microbial electron uptake in microbial electrosynthesis: a mini-review. J Ind Microbiol Biotechnol 46:1419–1426. https://doi.org/10.1007/s10295-019-02166-6

Keller R (2004) The computer aided resonance assignment tutorial. Pp. 1–81

Liu J, Wang Z, Belchik SM, Edwards MJ, Liu C, Kennedy DW, Merkley ED, Lipton MS, Butt JN, Richardson DJ, Zachara JM, Fredrickson JK, Rosso KM, Shi L (2012) Identification and characterization of MtoA: a decaheme *c*-type cytochrome of the neutrophilic Fe(II)-oxidizing bacterium *Sideroxydans lithotrophicus* ES-1. *In* Front Microbiol. Vol. 3. Pp. 37 https://doi.org/10.3389/fmicb.2012.00037

Low KO, Muhammad Mahadi N, Md Illias R (2013) Optimisation of signal peptide for recombinant protein secretion in bacterial hosts. Appl Microbiol Biotechnol 97:3811–3826. https://doi.org/10.1007/s00253-013-4831-z

Massey V (1959) The microestimation of succinate and the extinction coefficient of cytochrome *c*. Biochim Biophys Acta 34. https://doi.org/10.1016/0006-3002(59)90259-8

Morgado L, Salgueiro CA (2022) Elucidation of complex respiratory chains: a straightforward strategy to monitor electron transfer between cytochromes. *In* Metallomics. Vol. 14 https://doi.org/10.1093/mtomcs/mfac012

Piccioli M, Turano P (2015) Transient iron coordination sites in proteins: exploiting the dual nature of paramagnetic NMR. *In* Coordination Chemistry Reviews. Vol. 284. Pp. 313–328 https://doi.org/10.1016/j.ccr.2014.05.007

Querci L, Fiorucci L, Ravera E, Piccioli M (2024) Paramagnetic nuclear magnetic resonance: The Toolkit. *In* Inorganics. Vol. 12 https://doi.org/10.3390/inorganics12010015

Shen Y, Delaglio F, Cornilescu G, Bax A (2009) TALOS+: a hybrid method for predicting protein backbone torsion angles from NMR chemical shifts. *In* J Biomol NMR. Vol. 44. Pp. 213–23 https://doi.org/10.1007/s10858-009-9333-z

Silva AV, Louro RO (2017) Biomolecular NMR assignment: illustration using the heme signals in horse cytochrome *c*. *In* Journal of Chemical Education: American Chemical Society. Vol. 94. Pp. 1280–1284 https://doi.org/10.1021/acs.jchemed.7b00123

Summers ZM, Gralnick JA, Bond DR (2013) Cultivation of an obligate Fe(II)-oxidizing lithoautotrophic bacterium using electrodes. *In* mBio. Vol. 4. Pp. e00420-12 10.1128/mBio.00420–12

Thöny-Meyer L, Fischer F, Künzler P, Ritz D, Hennecke H (1995) *Escherichia coli* genes required for cytochrome *c* maturation. J Bacteriol Vol 177:4321–4326. https://doi.org/10.1128/jb.177.15.4321-4326.1995. *In*

Trindade IB, Coelho A, Cantini F, Piccioli M, Louro RO (2022) NMR of paramagnetic metalloproteins in solution: *Ubi venire,*

quo vadis?. J Inorg Biochem 234. https://doi.org/10.1016/j.jinorgbio.2022.111871

Ubbink M (2012) Dynamics in transient complexes of redox proteins. Biochem Soc Trans 40:415–418

Valdés J, Pedroso I, Quatrini R, Dodson RJ, Tettelin H, Blake R, Eisen JA, Holmes DS (2008) *Acidithiobacillus ferrooxidans* metabolism: from genome sequence to industrial applications. BMC Genomics Vol 9. https://doi.org/10.1186/1471-2164-9-597. *In*

Verissimo AF, Daldal F (2014) Cytochrome *c* biogenesis system I: an intricate process catalyzed by a maturase supercomplex? Biochim Biophys Acta 1837:989–998. https://doi.org/10.1016/j.bbabio.2014.03.003

Wishart DS, Bigam CG, Yao J, Abildgaard F, Dyson HJ, Oldfield E, Markley JL, Sykes BD (1995)) ^{1}H, ^{13}C and ^{15}N chemical shift referencing in biomolecular NMR. J Biomol NMR 6:135–140. https://doi.org/10.1007/s12104-014-9567-x

Zhong Y, Shi L (2018) Genomic analyses of the quinol oxidases and/or quinone reductases involved in bacterial extracellular electron transfer. Front Microbiol Vol 9. https://doi.org/10.3389/fmicb.2018.03029. *In*

Zhou N, Jessica K, Shawn LP, W. and, Chan Clara S (2022) Unraveling Fe(II)-oxidizing mechanisms in a facultative Fe(II) oxidizer, *Sideroxydans lithotrophicus* strain ES-1, via culturing, transcriptomics, and reverse transcription-quantitative PCR. *In* Applied and Environmental Microbiology: American Society for Microbiology. Vol. 88. Pp. https://doi.org/10.1128/AEM.01595-21